NANOSYSTEMS:
PHYSICS, CHEMISTRY, MATHEMATICS

Sudeshna Kar, Yian Tai *Nanosystems: Phys. Chem. Math.*, 2025, **16** (1), 74–88.
http://nanojournal.ifmo.ru
DOI 10.17586/2220-8054-2025-16-1-74-88

Original article

Isomeric protected dipeptides generated stable bio-compatible gold nanoparticles

Sudeshna Kar[1,2], Yian Tai[2]

[1]St. Thomas College of Engineering and Technology, Khidirpur, Kolkata, West Bengal 700023, Kolkata, India
[2]National Taiwan University of Science and Technology, 43 Keelung Road, Taipei-106, Taiwan

Corresponding author: Sudeshna Kar, 06.sudeshna@gmail.com; Yian Tai, ytai@mail.ntust.edu.tw

ABSTRACT It has been observed that two isomeric protected dipeptides which show altered nano-morphologies under similar conditions but behave unaltered to form stable gold nano-particles (AuNPs) having similar shape and size; whereas both the peptides showed fluctuating bio-compatibility but after conjugation with AuNP they show stable bio-compatibility. These gold nano conjugates are very stable, even up to 2 months the AuNPs showed no change in size or shape. Using a straightforward and reproducible one-pot synthetic technique, we were able to produce stable biocompatible gold nanoparticles using two isomeric protected dipeptides.

KEYWORDS bio-compatibility, isomeric dipeptides, one-pot synthesis, gold nano-particle, peptide-gold-nano-conjugates

ACKNOWLEDGEMENTS We acknowledge Tzu-Kuei Liu and Ming-Hua Ho of National Taiwan University of Science and Technology, Taiwan, for their generous help in doing the bio-compatibility test.

FOR CITATION Sudeshna Kar, Yian Tai Isomeric protected dipeptides generated stable bio-compatible gold nanoparticles. *Nanosystems: Phys. Chem. Math.*, 2025, **16** (1), 74–88.

Abbreviations

Gold nano-particles (AuNPs), 3-(4,5-dimethylthiazol-2-yl)-2,5-diphenyltetrazolium bromide (MTT), Sodium carbonate (Na_2CO_3)

1. Introduction

Peptides with the same brutto formula but distinct covalent structures are known as isomeric peptides. One of the most prevalent forms of positional isomerism among peptides that has been shown to significantly impact bioactivities is sequence reversal. For instance, it has been noted that alterations in the neurotoxicity of β-amyloid peptide (Aβ), the aggregation of which results in Alzheimer's disease, are brought about by a reversal of its sequence; for example, it has been discovered that the reverse copy of the highly neurotoxic β-amyloid peptide fragment Aβ(25–35), Aβ(35–25) is not neurotoxic [1]. Once more, there has been a noticeable difference in the biological activity of two antimicrobial peptides, Cecropin P (CP1) and its retro analogue, confirming that the peptide sequence determines the bioactivity of these peptides [2].

It has been observed that positional isomerism significantly alters the shape of peptides, which may significantly alter their biological activity [1, 3, 4]. It has been noted that the amino acids primarily responsible for the biological action of antimicrobial peptides are the N-terminal and C-terminal residues [5]. Since dipeptides are the smallest peptide fragments and can be produced at a lower cost than other options, they are our focus since they have demonstrated versatility in the creation of nanomaterials for use in nanobiotechnology [6–16]. In our previous work, it has been determined that the proper pairing of two conformationally rigid amino acids in isomeric dipeptides can result in a notable variation in self-assembly [17]. This can help to construct a variety of nanostructures under the same conditions, potentially modifying their biological activity [17]. These exceptional attributes motivated us to investigate the field of peptide research concerning isomeric peptides.

Peptide-gold nanoparticle (AuNP) conjugates are now a versatile tool for biomedical applications due to recent [18–20]. Peptides and gold nanoparticles are two potential material groups that can operate in accordance to enhance control over their respective biological functions and get beyond the inherent limitations of each material type alone. Gold nanoparticles (AuNPs) derived from self-assembling peptides have garnered significant attention and have been utilised in various scientific disciplines owing to their remarkable stability, biocompatibility, and activity [21, 22]. AuNP can be functionalized with peptides to prevent aggregation and facilitate their use in in-vitro and in-vivo applications [23]. Peptide-coated AuNP's extremely easy manufacturing, great stability, and biocompatibility have made it one of the most widely used biomaterials in recent years. The development of biosensors [24, 25], illness diagnosis [26, 27], and medicine have all benefited greatly from this [28, 29]. Previous studies have shown that smaller AuNP interact with cells more easily than larger nanoparticles, especially those with a diameter of 10 – 20 nm [30–35]. Sequential alterations in peptide-biphenyl hybrid ligands that cap spherical AuNP have been observed to provide a significant difference in biocompatibility

with the human hepatocellular cancer cell line Hep G2 when used at higher doses [36]. These noteworthy features drove us to study isomeric peptides in the realm of peptide research. As the two isomeric peptides "Boc-m-ABA-Aib-OMe" (Peptide I) and "Boc-Aib-m-ABA-OMe" (Peptide II) (Fig. 1(a, b)) showed different morphologies under identical condition due to different kind of self-assembly [17], we wanted to inspect how they interact with gold nanoparticle by reducing Chloroauric acid ($HAuCl_4$) and then capping the AuNPs. We also focused on the cell viability assay of the gold nanoparticles to see their bio-compatibility; we have created a straightforward, one-pot method to create very stable gold nanoparticles using these tiny protected di-peptides, which may be an effective substitute for chemical processes.

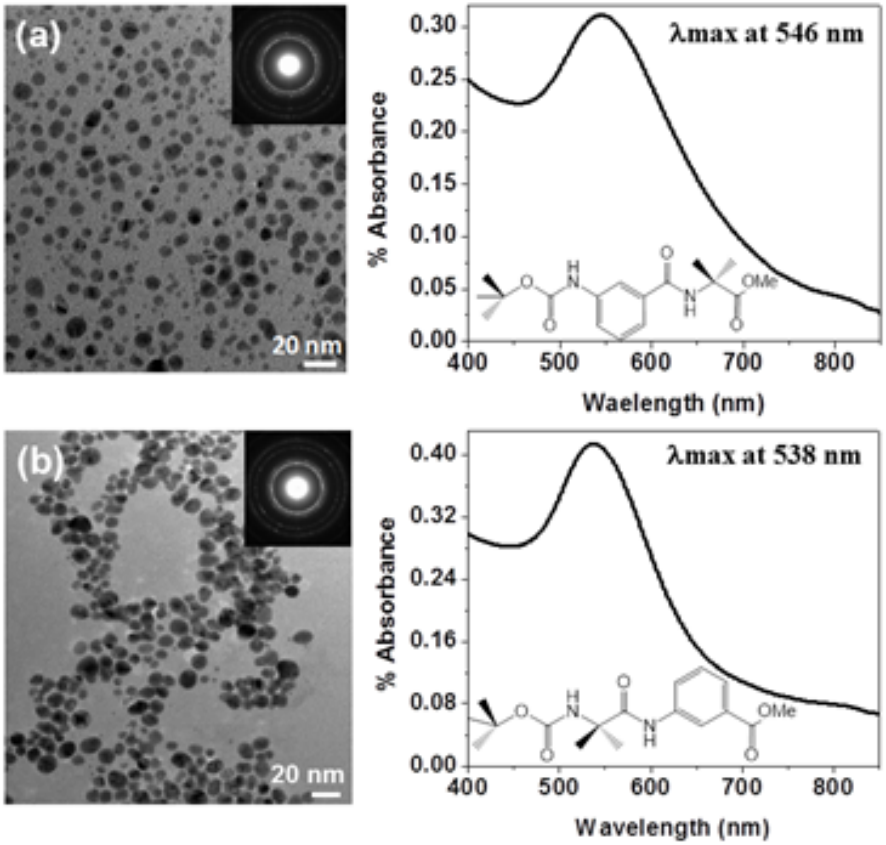

FIG. 1. (a) and (b) show TEM image and UV spectrum of peptide **I** and **II** bound AuNP solutions respectively; In the insets of (a) and (b) SAED pattern depict the polycrystalline nature of the AuNP; In the insets of UV spectra in (a) and (b) chemical structures of peptide **I** and **II** have been shown

2. Materials and methods

At first peptide **I** and **II** were synthesized in solution phase method; next with the help of these two peptide molecules gold nanoparticles were synthesized.

2.1. Methodology

2.1.1. Synthesis of Boc-mABA-OH. The amino acid *m*-aminobenzoic acid (6 g, 43.75 mmol) was suspended in a 1:1 tetrahydrofuran (THF) water mixture. Solid sodium bicarbonate $NaHCO_3$ (11.02 g, 131.25 mmol) was added and Boc-anhydride (10.49 ml, 48.12 mmol) was added to it. The reaction mixture was stirred at room temperature over night. After 24 h, the THF layer should be driven out with the help of vaccum pump. The aqueous layer was cooled in an icebath, acidified with 2 M HCl and extracted with ethylacetate. The organic layer was washed with excess of water and dried over anhydrous sodium sulphate, Na_2SO_4 and evaporated in *vacuo* producing a white solid. Yield: 9.20 g (88.71%).

2.1.2. Synthesis of methyl ester of a-aminoisobutyric acid (Aib-OMe). A mixture of absolute methanol (40 ml) and a-aminoisobutyric acid 1.5 g was cooled in an ice-salt bath for 30 mins. Then thionyl chloride (30 ml) was dropwise added to the reaction mixture with constant stirring and it was slowly allowed to attain room temperature. After stirring the clear mixture for 15 hrs. The excess methanol and thionyl chloride were removed and the residue was treated with ether. The solid methyl ester hydrochloride obtained (1.05 g) was dissolved in water, neutralised with sodium bicarbonate solution and extracted with ethyl acetate. Finally, the liquid ester was obtained by removal of solvent and it was used without further purification.

2.1.3. Synthesis of the peptide Boc-mABA-Aib-OMe (Peptide I) [17]. Boc-*m*ABA-OH was dissolved in dimethylformamide (1.25 g, 5.27 mmol) (DMF; 10 mL). N,N'-Dicyclohexylcarbodiimide, (DCC) (1.62 g, 7.90 mmol), Hydroxybenzotriazole, (HOBT) (1.6 g, 10.54 mmol), and methyl ester of 2-Aminoisobutyric acid Aib-OMe (1.6 g, 10.54 mmol) were then added (0.71 g, 5.27 mmol). During a whole day, the reaction mixture was stirred at room temperature. Filtered, then diluted with ethyl acetate, was the precipitated dicyclohexylurea (DCU) (80 mL). 100 mL of water, 1 M HCl (3×30 mL), 1 M sodium carbonate solution (3×30 mL), and then about 100 mL of water was used to wash the organic layer. A light-yellow gum was produced by drying the solvent over anhydrous sodium sulphate and allowing it to evaporate in vacuum. Silica gel was used as the stationary phase in the purification process, and a solution of ethyl acetate and petroleum ether served as the eluent. MeOH was used to generate single crystals that were stable at room temperature. 1.50 g (84.74 %) in yield. m.p. = 164 °C.

2.1.4. Synthesis of Boc-Aib-OH. The a-amino isobutyric acid (5 g, 48.54 mmol) was suspended in a 1:1 tetrahydrofuran (THF) water mixture. solid $NaHCO_3$ (12.23 g, 145.62 mmol) was added and Boc-anhydride (11.63 mL, 53.39 mmol) was added to it. The reaction mixture was stirred at room temperature over night. After 24 h, the THF layer should be driven out with the help of vaccum pump. The aqueous layer was cooled in an icebath, acidified with 2 M HCl and extracted with ethylacetate. The organic layer was washed with excess of water and dried over anhydrous Na_2SO_4 and evaporated in *vacuo* producing a white solid. Yield: 8.0 g (81.21 %).

2.1.5. Synthesis of methyl m-aminobenzoate (m-ABA-OMe). A mixture of absolute methanol (40 ml) and *m*-amino benzoic acid 1.37 g (10 mmol) was cooled in an ice-salt bath for 30 mins. Then thionyl chloride (30 ml) was dropwise added to the reaction mixture with constant stirring and it was slowly allowed to attain room temperature. After stirring the clear mixture for 15 hrs. the excess methanol and thionyl chloride were removed and the residue was treated with ether. The solid methyl ester hydrochloride obtained (1.03 g) was dissolved in water, neutralised with sodium bicarbonate solution and extracted with ethyl acetate. Finally, the liquid ester was obtained by removal of solvent and it was used without further purification.

2.1.6. Synthesis of the peptide Boc-Aib-mABA-OMe (Peptide II) [17]. Boc-Aib-OH was dissolved in dimethylformamide (0.65 g, 3.25 mmol) (DMF; 10 mL). Upon the addition of methyl ester of meta amino benzoic acid, *m*-ABA-OMe (1.40 g, 6.5 mmol) made from its hydrochloride, N,N'-Dicyclohexylcarbodiimide, DCC (0.97 g, 4.87 mmol), and Hydroxybenzotriazole, HOBT (0.42 g, 3.25 mmol). During a whole day, the reaction mixture was stirred at room temperature. Filtered, then diluted with ethyl acetate, was the precipitated dicyclohexylurea (DCU) (80 mL). 100 mL of water, 1 M HCl (3×30 mL), 1 M sodium carbonate solution (3×30 mL), and then about 100 mL of water was used to wash the organic layer. A light-yellow gum was produced by drying the solvent over anhydrous Na_2SO_4 and allowing it to evaporate in vacuum. Silica gel was used as the stationary phase in the purification process, and a solution of ethyl acetate and petroleum ether served as the eluent. 0.95 g (88.78 %) in yield. M.p = 138 °C.

2.1.7. Synthesis of gold nano particles (AuNPs). Separately, 0.84 mg/5 mL of peptides **I** and **II** were dissolved in 0.001 M chloroauric acid ($HAuCl_4$) solution, and the pH of both solutions was adjusted to ∼7 by adding 5 mL of 1.25 mM sodium hydroxide solution. The solution combinations were ultrasonically treated for five minutes in a special tank. The freshly created AuNPs solutions changed ruby red hue (Fig. A1, Appendix). Fourier transform infrared (FT-IR), X-ray energy dispersive spectrometric analysis (EDX), selected area diffraction pattern (SAED), transmission electron microscopic study (TEM), and proton nuclear magnetic resonance (^{1}H-NMR) spectroscopic investigation were used to describe the AuNP. Prior to performing the studies, we eliminated extra capping agent by ultrasonically dissolving AuNP deposits in extra MeOH and centrifuging the mixture. Every time, we eliminated the supernatant portion and carried out a second round of washing.

2.2. NMR Experiments

A Bruker Avance 300 model spectrometer running at 500 MHz was used to record all of the ^{1}H NMR spectra of the peptides and peptide bound AuNPs. In DMSO-D6, the peptide-bound AuNPs were dissolved.

2.3. FT-IR Spectroscopy

With a spectrophotometer of the Perkin Elmer-782 design, FT-IR spectra of PMM were studied. The KBr disc method was used to conduct the solid-state FT-IR measurements.

2.4. Transmission electron microscopic study

The morphology of the gold nanoparticles was examined using a transmission electron microscopic study (TEM) (AuNP). A drop of the appropriate solution was applied to a copper grid coated with carbon (300 mesh) for the TEM examinations of the peptide-AuNP, which was then slowly evaporated and allowed to dry under vacuum. TEM experiments were performed on these grids using a Philips Tecnai F20 G2 electron microscope. TEM pictures were captured at a 200 kV accelerated voltage. Also, the chosen area diffraction pattern allowed for the observation of the diffraction pattern

of a particular AuNP (SAED). X-ray energy dispersive spectrometry was also used to observe the qualitative elemental analysis (EDX).

2.5. UV-Vis analysis

Gold nanoparticles' surface Plasmon resonance (SPR) band was measured using a UV-Vis spectrophotometer. A JASCO V-670 spectrophotometer was used to record UV absorption spectra (800 – 200 nm).

2.6. In vitro cytotoxicity test using MTT assay

On a culture dish filled with cell medium (a mixture of 90 % Dulbeco's modified eagle's medium, 10 % foetal bouvine serum, and 1 mM sodium pyruvate), osteoblast type 7F2 cells (derived from mouse bone marrow) were sown at a density of 12000 cells per millilitre for 24 hours to allow for cell growth. After the full development of the cells, 450 L of cell media and 50 L of a peptide bound AuNPs solution (5 μg/mL) were added to each well, and the cells were then incubated for 1, 3 and 5 days. Similar experiments were performed with peptide **I** and **II** also with the same concentration (5 μg/mL). For the purpose of observing cell vitality, MTT (3-(4,5-dimethylthiazol-2-yl)-2,5-diphenyltetrazolium bromide) was applied to the cell-well after 1, 3 and 5 days. MTT is converted into a purple formazan product with a maximum absorbance near 570 nm by viable cells with an active metabolism. The MTT tetrazolium's formazan product deposits near the cell surface, inside cells, and in the culture medium as an insoluble precipitate. Before taking readings on absorbance, the formazan is solubilized in DMSO. The quantity of live cells is likely directly correlated with the formazan absorbance at 570 nm using a plate reading spectrophotometer (OD value at 570 nm).

2.7. Zeta potential measurements

According to the manufacturer's instructions, the zeta potentials of solutions of gold nanoparticles in water were measured. A Brookhaven Instruments Company Zeta Potential Analyzer was used for the analysis. Direct placement of gold nanoparticle solutions into a cuvette with a zeta potential electrode within was used. It was believed that only the gold nanoparticles would produce results from the zeta potential experiments. In order to measure the peptides, a zeta potential electrode was placed within a cuvette containing a methanolic solution of both peptides (0.84 mg/5 mL) (Table A1 in Appendix)

3. Results and discussions

Both peptide molecules formed spherical AuNP, as seen in TEM images (Fig. 1(a,b)). AuNP's diameters were in the 10 – 20 nm range, which is ideal for cellular uptake (Fig. 1(a,b)) [13–16]. The polycrystalline character of the AuNP was represented by the SAED pattern (insets of Fig. 1(a,b)). A distinctive peak for spherical AuNP, the surface plasmon resonance (SPR) bands for peptide **I** conjugated AuNP and peptide **II** conjugated AuNP are found at 546 and 538 nm, respectively (Fig. 1(a,c)) [25–28]. Using "Image J" software, we determined the sizes of the spherical gold nanoparticles from a fraction of the TEM pictures. 150 nanoparticles' worth of data was gathered, and the size distribution profile was displayed in origin while the mean standard deviation was computed. The average diameter of spherical AuNPs produced by peptide **I** was predicted to be 4.4 ± 1.2 nm, whereas the average diameter of AuNPs bound to peptide **II** was discovered to be 8.8 ± 2.25 nm. Fig. 2 depict the size distribution profile for peptide bound AuNPs.

In addition to the C, N, and O that the peptide molecules contributed, the Energy dispersive X-ray (EDX) examination also amply demonstrates the existence of gold nanoparticles on the surface of AuNP (Fig. 3).

We carried out Fourier-transform infrared (FT-IR) experiments to investigate the chemical interactions between the peptides and AuNP [25–28]. FT-IR spectrum of Peptide **I** shows a band at 3347.43 cm^{-1} caused by N–H stretching vibrations as well as a broad band at 3251.65 – 3271.6 cm^{-1} (Shoulder band, which is an overtone of the N–H bending vibration). Nevertheless, peptide **I** coupled with gold nanoparticles showed an N–H stretching frequency of 3394.42 and 3347.13 cm^{-1} (Fig. 4).

The interaction of the –NH group in the amide bond with gold can be used to explain the increase in wavenumber. The overtone 3251.65 – 3271.6 cm^{-1} discovered in the single peptide molecule can't be found may be due to interaction of AuNP with peptide **I**. Peak positions did not significantly alter for the C=O stretching frequency range (Fig. 5). A new peak was discovered for peptide **II**-bound AuNP at location 3442.91 cm^{-1} in addition to peak 3324.5, which also revealed a strong interaction between the –NH group in the amide bond and gold (Fig. A2, Appendix). In the range of C=O stretching (Fig. A3, Appendix), no appreciable change in peak position was seen either.

We used a ^{1}H-NMR spectroscopy investigation to further confirm and pinpoint the precise chemical interaction between peptide molecules and AuNP [29]. The signal for the C-terminal amino acid, Aib-NH, appeared at 8.527 ppm and was displaced to 8.306 ppm following conjugation with AuNP, while the peak for the N-terminal amino acid, *m*-ABA-NH, appeared at 9.446 ppm for peptide **I** in D6-dimethyl sulfoxide solvent (Table 1 and Figs. 6 and 7). By interactions with arene-cations (metals), the presence of aromatic rings in the *m*-ABA residue can also help stabilize the nanoparticle [28]. Both a reducing and a capping effect are possible with *m*-ABA [25–31]. Due to this, both the up-field and down-field shifts, which are modest relative to the N–H shifts, were observed in the aromatic C-H area, specifically between 7 ppm and 8 ppm (Figs. 6 and 7).

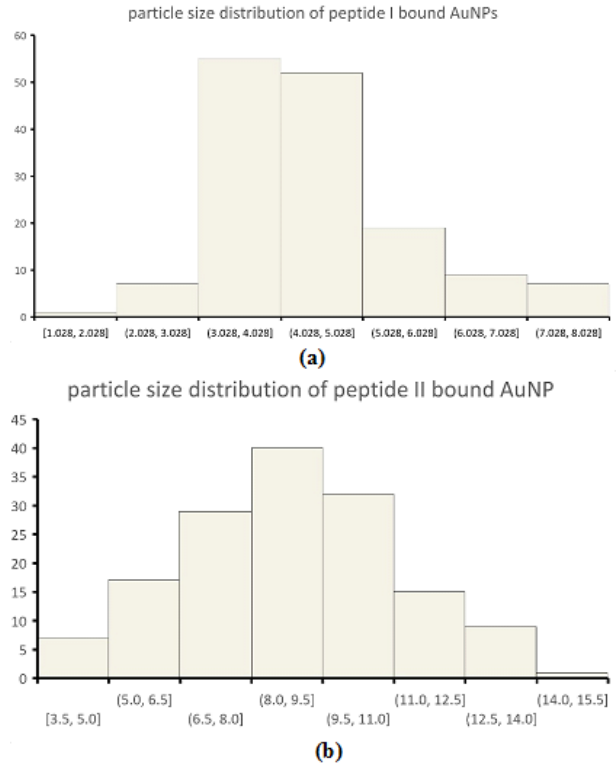

FIG. 2. Particle size distribution of (a) peptide **I** bound AuNPs and (b) Particle size distribution of peptide **II** bound AuNPs

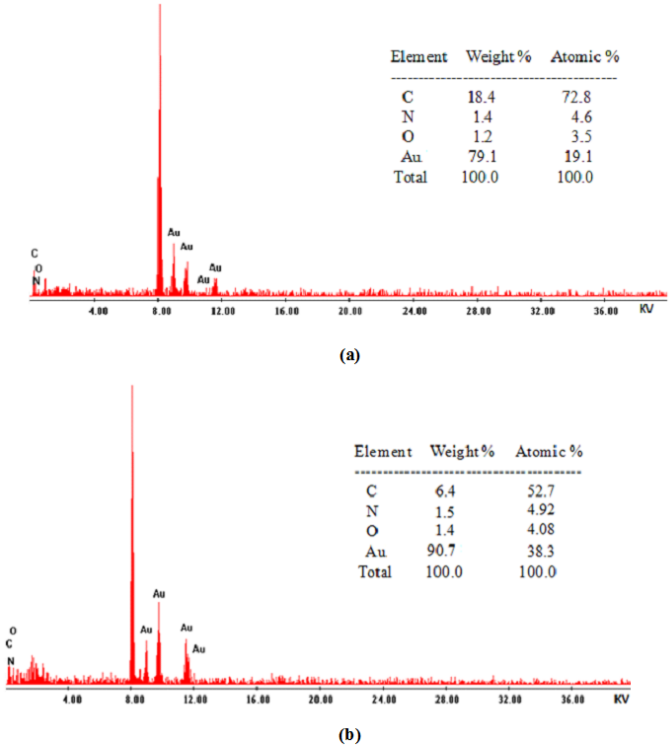

FIG. 3. EDX analysis of AuNPs synthesized by (a) peptide **I** and (b) peptide **II**. EDX analysis clearly indicates the presence of Au nanoparticle along with C, N and O contributed by the peptide molecules on the surface of AuNPs

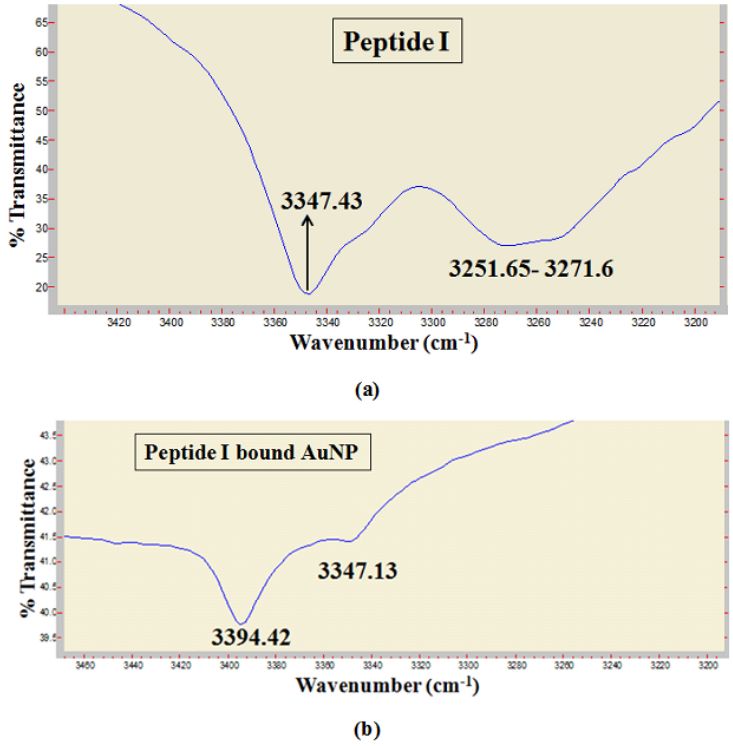

FIG. 4. FT-IR spectra of (a) peptide **I** and (b) peptide **I** bound gold nano-particles (AuNPs) in solid state (3200 – 3430 cm^{-1} range)

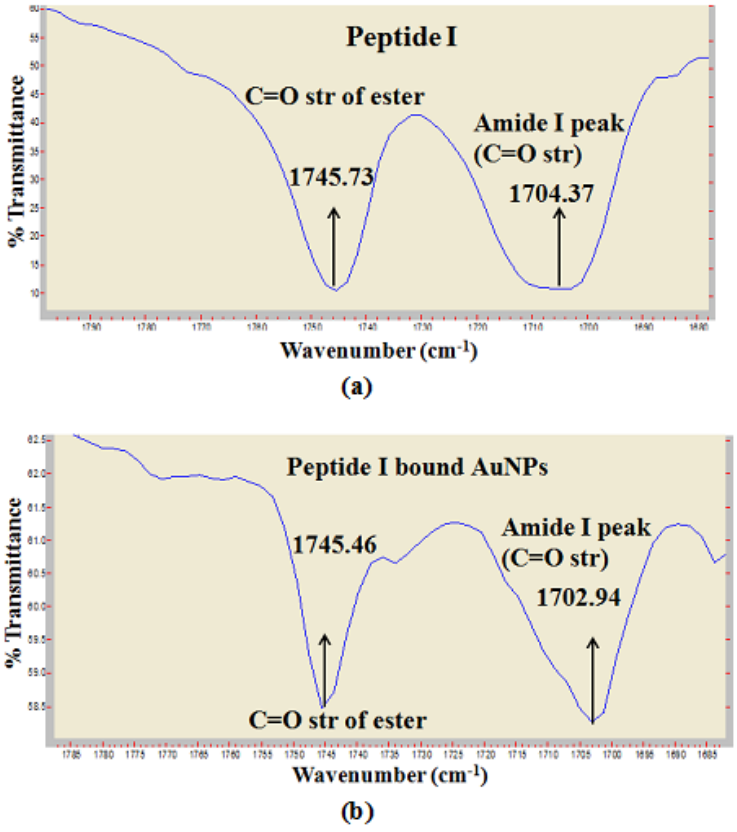

FIG. 5. FT-IR spectra of (a) peptide **I** and (b) peptide **I** bound gold nano-particles (AuNPs) in solid state (1680 – 1780 cm^{-1} range)

TABLE 1. Comparison of ^{1}H NMR Chemical Shift Values (in PPM) of Peptides and Peptide Bound AuNP (In DMSO-D6 (500 MHz))

Functional group	Peptide I	Peptide I AuNP	Peptide II	Peptide II AuNP
***m*ABA-NH**	9.446	9.698	9.685	9.445
Aib-NH	8.527	8.306	8.297	8.527
-OCH$_3$	3.582	3.847	3.847	3.582

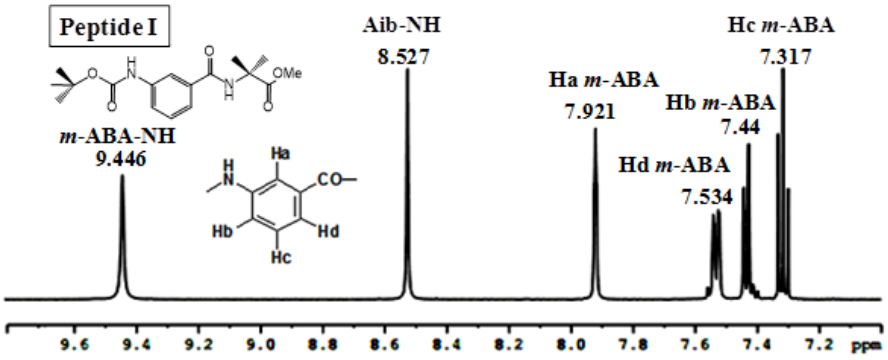

FIG. 6. ^{1}H NMR spectrum of peptide **I** in DMSO-D6 (500 MHz) (7 – 10 ppm region)

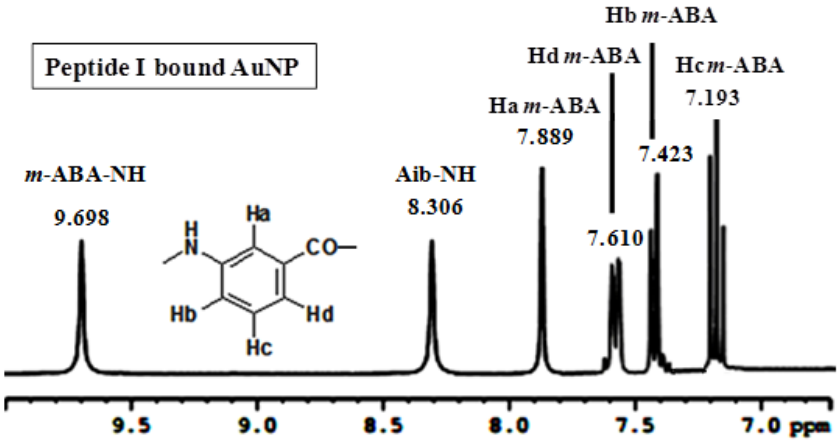

FIG. 7. ^{1}H NMR spectrum of peptide **I** bound AuNPs in DMSO-D6 (500 MHz) (7 – 10 ppm region)

After conjugation with AuNP, the ^{1}H-NMR peak for –OCH$_3$ in peptide **I** changed to 3.847 ppm from 3.582 ppm (Table 1 and Figs. 8 and 9). It follows that oxygen in the –OCH$_3$ group contributes electrons to the reduction of Au^{3+}. Moreover, the Boc-CH3 ^{1}H-NMR signal was at 1.477 ppm prior to conjugation with AuNP and shifted to 1.295 ppm following conjugation (Figs. 8 and 9). After conjugation with AuNP, the peak for C–H of Aib hardly migrated to the up-field area (from 1.444 to 1.375 ppm) (Figs. 8 and 9).

Curiously, the pattern of NMR peak shifts corresponding to individual amino acids differs from that of peptide **I** after binding with AuNP in the instance of peptide **II**, which is a positional isomer of peptide **I** with the position of *m*-ABA and Aib inverted. Whereas Aib-NH occurred at 8.297 ppm for peptide **II** and was pushed down field to 8.527 ppm after conjugation with AuNP, the peak for *m*-ABA-NH appeared at 9.685 ppm for peptide **II** was shifted up field to 9.445 ppm (Table 1 and Figs. A4 and A5 in Appendix). As a result, when peptide **II** is attached to AuNP, *m*-ABA acts as a capping agent, which is seen as an "up field" shift in the aromatic C–H region (between 7 and 8 ppm; Figs. A4 and A5 in Appendix), and Aib acts as a reducing agent, which is visible as a "down field" shift (Figs. A4 and A5, Appendix). After conjugation with AuNP, the ^{1}H-NMR signal for –OCH$_3$ in peptide **II** was moved up field to 3.582 from 3.847 ppm (Table 1 and Figs. A6 and A7 in Appendix). Moreover, the ^{1}H-NMR signal for Boc-CH$_3$ was displaced from 1.377 to

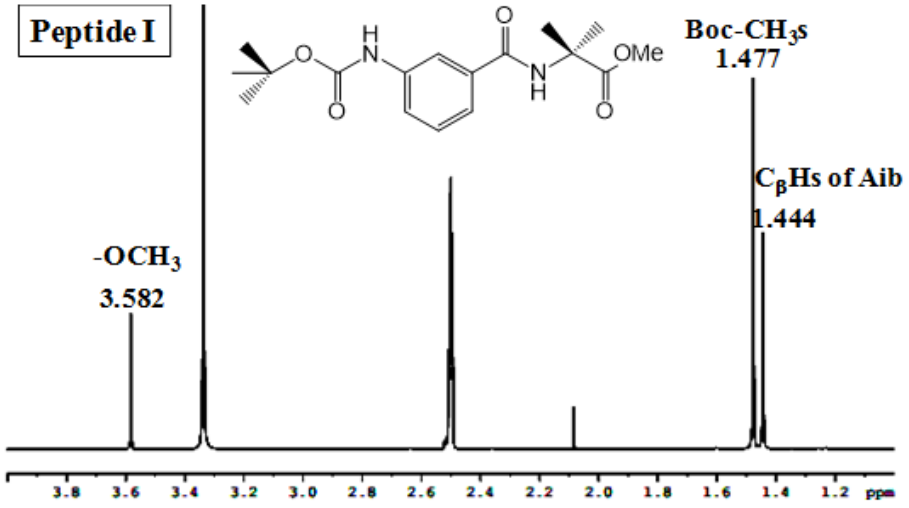

FIG. 8. ^{1}H NMR spectrum of peptide **I** in DMSO-D6 (500 MHz) (1 – 4 ppm region)

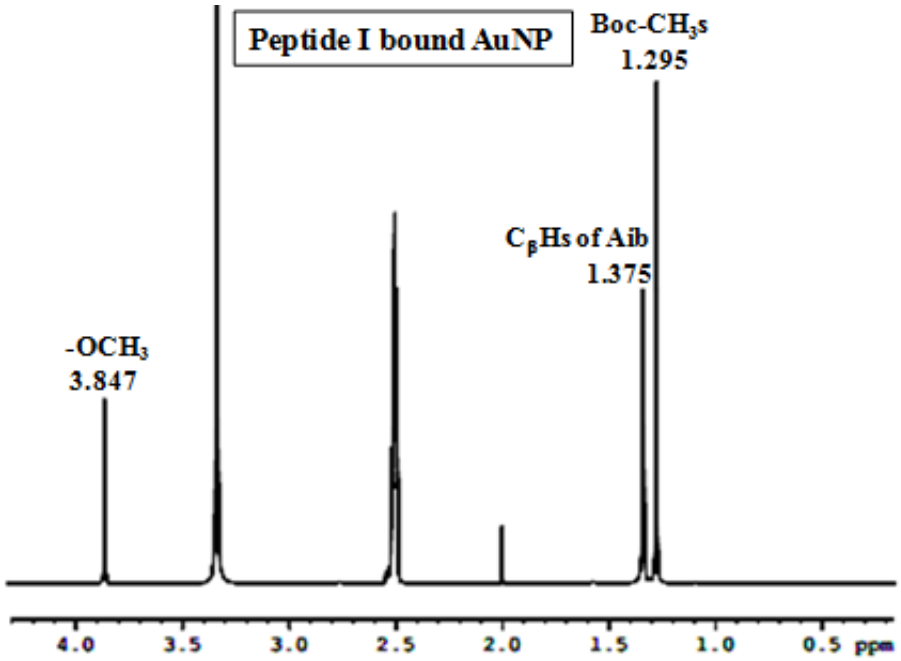

FIG. 9. ^{1}H NMR spectrum of peptide **I** bound AuNPs in DMSO-D6 (500 MHz) (1 – 4 ppm region)

1.476 ppm following conjugation with AuNP (Figs. A6 and A7, Appendix). Together, the results of the ^{1}H-NMR study led us to hypothesis that in these peptide molecules, the N-terminal amino acid is in charge of reducing the Au^{3+} ion by accepting electrons from nitrogen and the C-terminal amino acid is in charge of capping AuNP by donating as well as accepting electrons to gold. The NMR shifts of additional segments or groups connected to the relevant amino acids also reflect this. Hence, during the production of metal nanoparticles, the position of amino acids has a significant impact on the ability to donate and absorb electrons.

The AuNP solutions were kept at room temperature for two months to test their stability. After two months, we found no precipitation or colour change in the solution. UV-Vis absorption spectra of AuNP solutions after two months of storage were gathered and contrasted with those of freshly generated AuNP solutions to ensure that there is no aggregation. Figs. A8(a,c) (Appendix) of the spectra show no discernible change in the plasmon absorption bands, demonstrating the absence of nanoparticle aggregation in the solution [32]. According to TEM images of 2-month-old peptide-bound AuNP, neither the form nor the size of the AuNP had changed (Fig. A8(b,d), Appendix). We can infer that the absence of any free functional groups in the peptide molecules lowers the likelihood that the peptide bound AuNP will aggregate, limiting the interactions between the peptides and promoting the production of stable AuNP. Consequently, we have created a straightforward, one-pot method to create very stable gold nanoparticles using tiny protected di-peptides, which may be an effective substitute for chemical processes.

Following that, cell survival assays were conducted using gold nanoparticles that had been stabilized with peptides **I** and **II** and had similar size and shape. With the MTT assay, we were able to monitor the cell survival of the peptides and peptide-bound AuNP towards osteoblast type 7F2 cells (derived from mouse bone marrow) for up to 5 days [33–36]. Because they allow for bone formation, remodelling, and repair, osteoblasts are crucial. It was shown that cell viability fluctuated when both peptides were present, suggesting that both peptides randomly interact with normal cells (Fig. 10 and Table A2 in Appendix). The isomeric structure of peptides **I** and **II** refers to their comparable content but different sequencing. The fact that both peptides position themselves around each cell in a way that creates an extracellular matrix with a lot of good binding sites may be the cause. Both peptides are small in size, flexible, and interact with cells randomly, which occasionally encourages cell spreading and allows for prolonged cell viability. However, occasionally due to improper orientation of the peptide molecules, proper binding with the cells may not be facilitated and cell spreading may not be permitted. In contrast, MTT results for peptide **I** and peptide **II** bound AuNP were significantly stable when applied to normal bone cells (Fig. 10 and Table A2 in Appendix). After 1, 3, and 5 days, it was shown that cell viability in the presence of peptide **II** bound AuNP was marginally lower than that of peptide **I** bound AuNP. That may be because of the following factors.

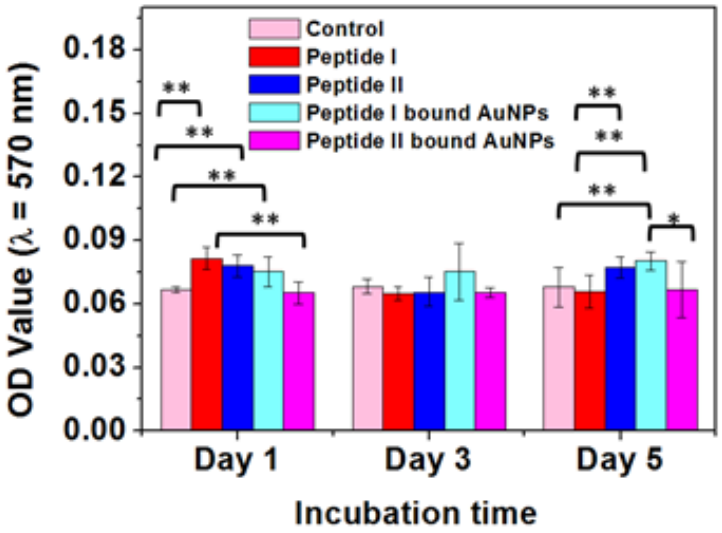

FIG. 10. MTT assay for peptide **I**, **II** and peptide bound AuNP. Methanol water (1:1 v/v) was used as the control system. The absorbance of formazan at 570 nm using a plate reading spectrophotometer (OD value at $l = 570$ nm) is presumably directly proportional to the number of viable cells. (*) means significant difference (0.01 – 0.05) and (**) means very significant difference (0.001 – 0.01)

First, even though the peptide-bound AuNPs' sizes and shapes are relatively similar, their distributions varied slightly. It was discovered that the number density of peptide **II** bound AuNP was lower than that of peptide **I** bound AuNP (Fig. 1). This distributional difference may have an impact on how well the two peptide bound AuNPs are absorbed by cells and affect cell survival. Second, if we look at the schematics for both peptides, we can see that N3 and N4 are separated by a flexible group like $–C(CH_3)_2$, while N1 and N2 are separated by a hard group, the phenyl ring (Fig. 11). The –NH– groups' ability to adhere to the surface of Au may be partially inhibited by these steric effects, which would affect their capacity to be cytotoxic. On the other hand, it is evident that for both peptides, the fluctuation of cell viability decreases after binding with AuNP; this may be because a portion of the peptides' binding sites are involved in capping the AuNP and as a result, fewer binding sites are available to interact with cells. As a result, there is less fluctuation in cell viability since the randomness of the peptides' binding to the cell is reduced. We draw the conclusion that the peptide-bound AuNPs are displaying slight difference in cell viability since we see a noticeable difference in standard deviation values and the pairwise t-test also reveals a significant difference between means.

One of the key physical factors affecting AuNP toxicity is surface charge, as determined by zeta potential [37]. It is crucial to keep in mind that modifying NP surfaces could result in different ionic interactions with biological systems because surface charges can alter [38, 39]. Mean zeta potentials (ζ-potentials) of peptide **I** attached AuNP solutions were determined to be $+12.47 \pm 1.67$ and $+6.97 \pm 1.63$ mV, respectively. Experimental parameters have been mentioned in Table A1 (Appendix).

Without AuNP conjugation, the zeta potentials of peptides **I** and **II** were likewise measured to be -7.17 ± 0.38 and -8.37 ± 0.63 mV, respectively. Two peptides' negative zeta-potentials were changed to positive ones after conjugation with AuNP, probably as a result of the electron-rich groups responsible for showing negative ζ-potential on the peptides being bound to the surface of AuNP. We presume that the conjugates become positively charged because we have already

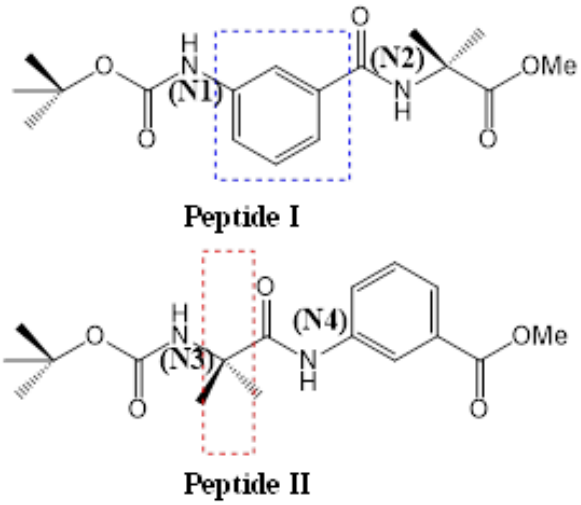

FIG. 11. Schematic representation of peptide **I** and peptide **II**

shown that peptide molecules work as the reducing agent to generate the AuNP by donating electrons from nitrogen and oxygen present in various groups. Spectroscopic studies have already shown that the role of amino acids in reducing Au^{3+} and capping the AuNP has changed because of changes in amino acid position in the peptide sequence. Hence, it stands to reason that this phenomenon will have an impact on how the peptides **I** and **II**, which act as capping agents, are distributed in bulk on the AuNP, changing their +ve ζ-potential. A positive ζ-potential not only offers advantages for improved DNA loading efficiency but may also give the effective accumulation in the target cells since many proteins, DNA, and cell membrane surfaces are somewhat anionic [40]. Because cationic nanoparticles are an easy, safe, and effective route to transport medicinal chemicals, more and more researchers are now using them [41].

4. Conclusion

In conclusion, using a straightforward and reproducible one-pot synthetic technique, we were able to produce stable gold nanoparticles using two isomeric peptides molecules having no free functional group. We demonstrated that despite the similar composition of these isomeric peptides, they show fluctuating cell-viability effects [17], which decreases after conjugation with gold nanoparticles. Moreover, following binding with AuNP, the isomeric peptides exhibits very stable and reliable MTT assay even after prolonged incubation with normal cells, making them more biocompatible. Our spectroscopic investigations show that amino acids' roles in reducing Au^{3+} and capping the AuNP are altered because of changes in amino acid position in the peptide sequence. After all the experiments we performed, it has been observed that two isomeric dipeptides which show altered nano-morphologies under similar conditions but behave unaltered to form AuNPs having similar shape and size; whereas both the peptides showed fluctuating bio-compatibility but after conjugation with AuNP they show stable bio-compatibility. Therefore we can conclude, although two isomeric peptides undergo different self-assembly pattern to develop different morphological pattern but in case of forming gold nanoparticle they behave as individual peptide molecule. These peptides capped nanoparticle may facilitate the binding of other biologically active proteins on their surface by protein-peptide interaction, for model study. Isomeric peptide bound AuNPs may bind with the same protein molecule differently, which there-by can cause different functionality of the same protein molecule which may find its' use in nanomedical devices and therapeutics development. Some crucial benefits of using these peptide-conjugated-gold-nanoparticles might be enhanced specificity, increased penetration, improved solubility and reduced toxicity. By binding with specific bioactive peptides which inhibit any disease can enhance the inhibition process and will minimize off-target effects reducing the risk of damaging healthy cells. The small size of peptide bound AuNPs can allow them to penetrate through blood-brain barrier and reach the brain more effectively, facilitating the delivery of therapeutic agents to the target site; the hydrophobic nature of some neurodegenerative disease-creating peptide-folding makes them especially difficult to dissolve in aqueous solutions, limiting the efficacy of traditional drug delivery methods; these peptide bound AuNPs can be engineered to enhance the solubility of drugs, facilitating their delivery to the target site; these AuNPs can improve the pharmacokinetic and pharmacodynamic properties of therapeutic agents, reducing their toxicity and improving their therapeutic index. Another important aspect of using peptide bound AuNPs is that these are very stable, even up to 2 months the AuNPs showed no change in size or shape. This factor is very important for use of AuNPs in biological field for their efficiency and safety issue.

Appendix

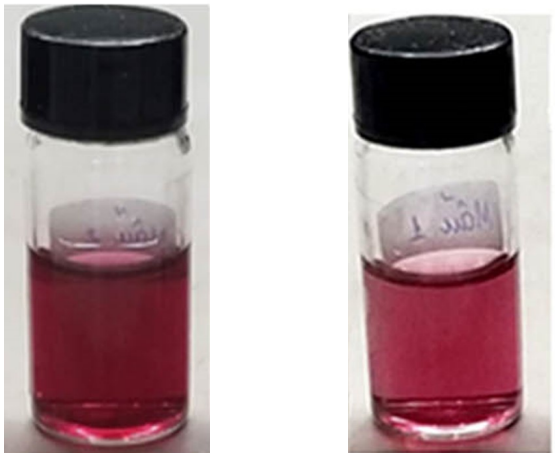

Peptide **I** bound AuNPs Peptide **II** bound AuNPs

FIG. A1. The color of the newly synthesized AuNPs solutions

TABLE A1. Experimental parameters of Zeta potential study

Measurement Parameters:			
		Liquid	= Methanol
Zeta Potential Model	= Smoluchowski	Temperature	= 25.0 °C
Mean Mobility	= 1.01 (μ/s) / (V/cm)	Viscosity	= 0.548 cP
pH	= 7.00	Refractive Index	= 1.324
Conductance	= 248 μS	Dielectric Constant	= 32.63

Instrument Parameters:			
Sample Count Rate	= 375 kcps	Voltage	= 4.00 volts
Ref. Count Rate	= 1263 kcps	Electric Field	= 7.36 V/cm
Wavelength	= 659.0 nm		
Field Frequency	= 2.00 Hz		
Cycles Per Run	= 20		

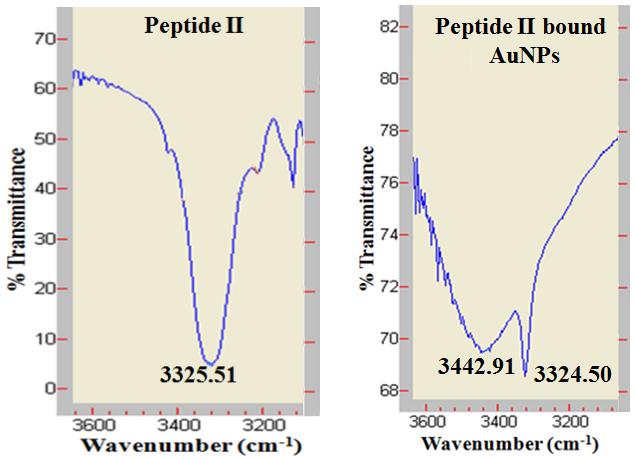

FIG. A2. FT-IR spectra of peptide **II** and peptide **II** bound gold nano-particles (AuNPs) in solid state (3200 – 3600 cm^{-1} range)

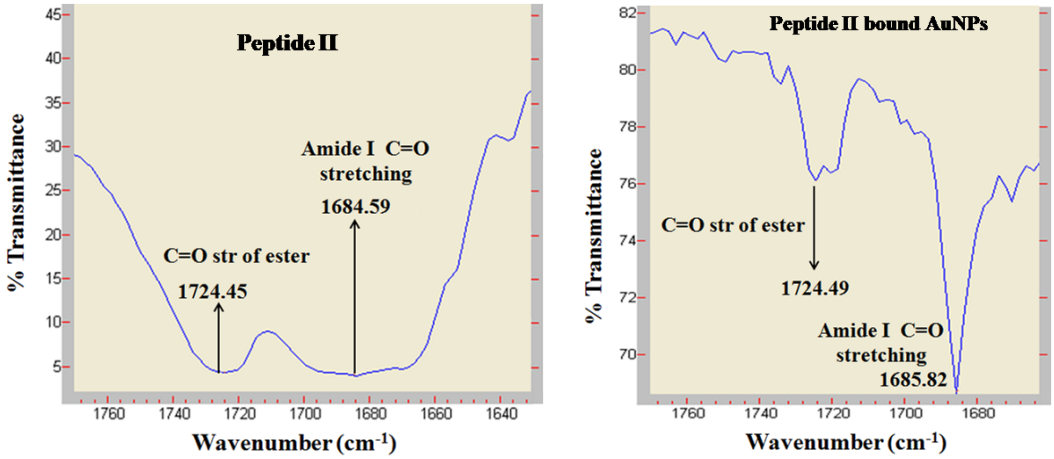

FIG. A3. FT-IR spectra of peptide **II** and peptide **II** bound gold nano-particles (AuNPs) in solid state (1640 – 1760 cm^{-1} range)

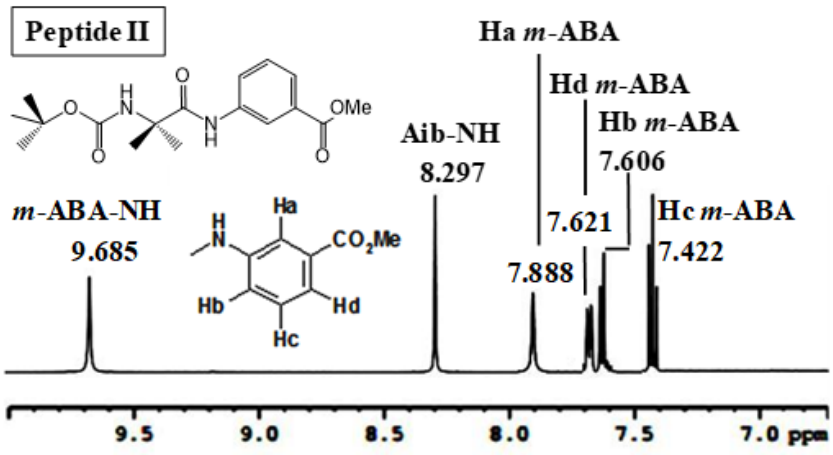

FIG. A4. ^{1}H NMR spectrum of peptide **II** in DMSO-D6 (500 MHz) (7 – 10 ppm region)

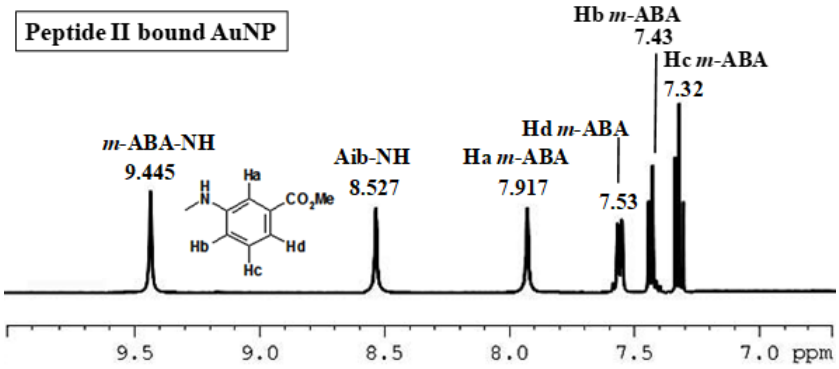

FIG. A5. ^{1}H NMR spectrum of peptide **I** bound AuNPs in DMSO-D6 (500 MHz) (7 – 10 ppm region)

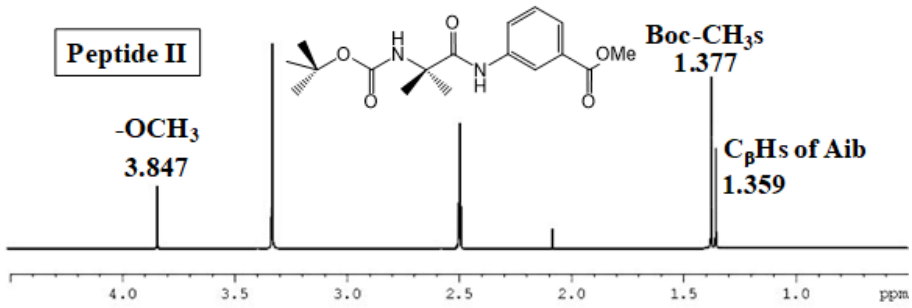

FIG. A6. ^{1}H NMR spectrum of peptide **II** in DMSO-D6 (500 MHz) (1 – 4 ppm region)

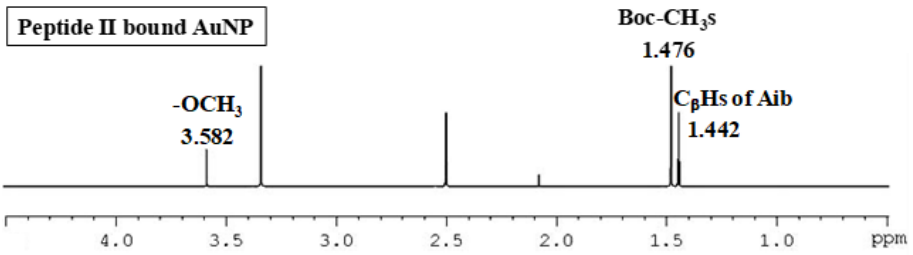

FIG. A7. ^{1}H NMR spectrum of peptide **II** bound AuNPs in DMSO-D6 (500 MHz) (1 – 4 ppm region)

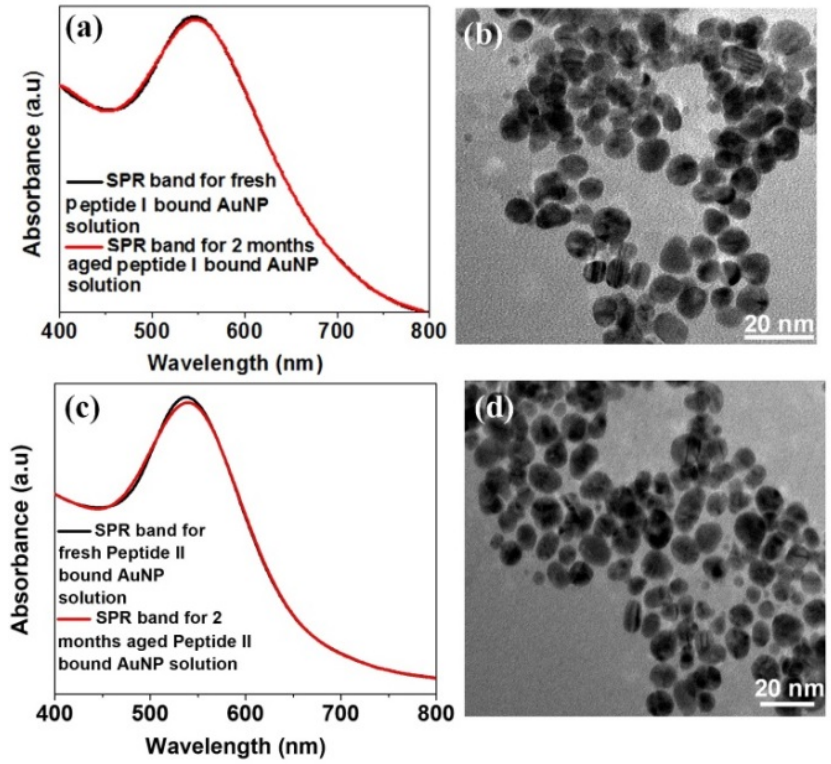

FIG. A8. (a) surface plasmon resonance band for freshly prepared peptide **I** bound AuNP solution and 2 months aged peptide **I**/AuNP solution are shown in the UV spectrum; (b) TEM image of 2 months aged peptide **I**/AuNP; (c) surface plasmon resonance band for freshly prepared peptide **II** bound AuNP solution and 2 months aged peptide **II**/AuNP solution are shown in the UV spectrum; (d) TEM image of 2 months aged peptide **II**/AuNP

TABLE A2. Statistical results of MTT test

Sample	Control	Peptide I	Peptide II	Peptide I AuNP	Peptide II AuNP
Day 1	0.067 ±0.002	0.082 ± 0.005	0.078 ± 0.006	0.075 ± 0.008	0.065 ± 0.007
Day 3	0.068 ±0.003	0.065 ±0.003	0.066 ± 0.007	0.075 ± 0.014	0.065 ± 0.002
Day 5	0.068 ± 0.010	0.066 ± 0.008	0.077 ± 0.005	0.08 ± 0.005	0.067 ± 0.013

References

[1] Butterfield D.A., Hensley K., Harris M., Mattson M., Carney J. β-Amyloid Peptide Free Radical Fragments Initiate Synaptosomal Lipoperoxidation in a Sequence-Specific Fashion: Implications to Alzheimer's Disease. *Biochem. Biophys. Res. Commun.*, 1994, **200**, P. 710–715.

[2] Vunnam S., Juvvadi P., Merrifield R.B. Synthesis and antibacterial action of cecropin and proline-arginine-rich peptides from pig intestine. *J. Pept. Res.*, 1997, **49**, P. 59–66.

[3] Marqusee S., Baldwin R.L. Helix stabilization by Glu-...Lys+ salt bridges in short peptides of de novo design. *Proc. Natl. Acad. Sci. U. S. A.*, 1987, **84**, P. 8898–8902.

[4] Bond, J.P., Deverin, S.P., Inouye, H., El-Agnaf O.M.A., Teeter M.M., Kirschnera D.A. *J. Struct. Biol.*, 2003, **141**, P. 156–170.

[5] Soares J.W., Mello C.M. Antimicrobial Peptides: a Review of How Peptide Structure Impacts Antimicrobial Activity. *Proceedings of SPIE*, 2004, **5271**, P. 20–27.

[6] Yang Z.M., Gu H., Zhang Y., Wang L., Xu B. Small molecule hydrogels based on a class of antiinflammatory agents. *Chem. Commun.*, 2004, **9**, P. 208–209.

[7] Reches M., Gazit E. Formation of closed-cage nanostructures by self-assembly of aromatic dipeptides. *Nano Lett.*, 2004, **4**, P. 581–585.

[8] Yan X., Zhu P., Li J. Self-assembly and application of diphenylalanine-based nanostructures. *Chem. Soc. Rev.*, 2010, **39**, P. 1877–1890.

[9] Wang W., Yang Z., Patanavanich S., Xu B., Chau Y. Controlling self-assembly within nanospace for peptidenanoparticle fabrication. *Soft Matter*, 2008, **4**, P. 1617–1620.

[10] Toledano S., Williams R.J., Jayawarna V., Ulijn R.V. Enzyme-Triggered Self-Assembly of Peptide Hydrogels via Reversed Hydrolysis. *J. Am. Chem. Soc.*, 2006, **128**, P. 1070–1071.

[11] Reches M., Gazit E. Enzyme-Triggered Self-Assembly of Peptide Hydrogels via Reversed Hydrolysis. *Nat. Nanotechnol.*, 2006, **1**, P. 195–200.

[12] Laromaine A., Koh L., Murugesan M., Ulijn R.V., Stevens M.M. Protease-Triggered Dispersion of Nanoparticle Assemblies. *J. Am. Chem. Soc.* , 2007, **129**, P. 4156–4157.

[13] Reches M., Gazit E. Casting metal nanowires within discrete self-assembled peptide nanotubes. *Science*, 2003, **300**, P. 625–627.

[14] Amdursky N., Koren I., Gazit E., Rosenman G. Adjustable Photoluminescence of Peptide Nanotubes Coatings. *J. Nanosci. Nanotechnol.*, 2011, **11**, P. 9282–9286.

[15] Carny O., Gazit E. Creating prebiotic sanctuary: Self-assembling supramolecular peptide structures bind and stabilize RNA. *Origins Life Evol. Biospheres*, 2011, **41**, P. 121–132.

[16] Yemini M., Reches M., Rishpon J. Gazit E. Novel electrochemical biosensing platform using self-assembled peptide nanotubes. *Nano Lett.*, 2005, **5**, P. 183–186.

[17] Kar S., Tai Y. Marked difference in self-assembly, morphology and cell viability of positional isomeric dipeptides generated by reversal of sequence. *Soft Matter.*, 2015, **11**, P. 1345–1351.

[18] Goddard Z.R, Beekman A.M., Cominetti M.M.D., O'Connell M.A., Chambrier I., Cook M.J., Marín M.J., Russell D.A., Searcey M. Peptide directed phthalocyanine-gold nanoparticles for selective photodynamic therapy of EGFR overexpressing cancers. *RSC Med. Chem.*, 2021, **12**, P. 288–292.

[19] Rai A., Ferreira L. Biomedical applications of peptide decorated gold nanoparticles. *Critical Reviews in Biotechnology*, 2021, **41**, P. 186–215.

[20] Kumar A., Ma H., Zhang X., Huang K., Jin S., Liu J., Wei T., Cao W., Zou G., Liang X.J. Gold nanoparticles functionalized with therapeutic and targeted peptides for cancer treatment. *Biomaterials*, 2012, **33**, P. 1180–1189.

[21] Bucci R., Maggioni D., Locarno S., Ferretti A.M., Gelmi M.L., Pellegrino S. Exploiting ultrashort a,b-peptides in the colloidal stabilization of gold nanoparticle. *Langmuir*, 2021, **37**, P. 11365–11373.

[22] Li Y., Tang Z., Prasad P.N., Knecht M.R., Swihart M.T. Peptide-mediated synthesis of gold nanoparticles: effects of peptide sequence and nature of binding on physicochemical properties. *Nanoscale*, 2014, **6**, P. 3165–3172.

[23] Kalimuthu K., Lubin B.C., Bazylevich A., Gellerman G., Shpilberg O., Luboshits G., Firer M.A. Gold nanoparticles stabilize peptide-drug-conjugates for sustained targeted drug delivery to cancer cells. *Nanobiotechnol.*, 2018, **16**, 34.

[24] Zhao X.R., Chen Y.L., Wang L., Wang W.F., Chen X.G. Highly sensitive fluorescence detection of trypsin based on gold nanoparticle probe. *Anal. Methods*, 2016, **8**, P. 393–400.

[25] Chandrawati R., Stevens M.M. Controlled assembly of peptide-functionalized gold nanoparticles for label-free detection of blood coagulation factor XIII activity. *Chem. Commun.*, 2014, **50**, P. 5431–5434.

[26] Liu X., Wang Y., Chen P., McCadden A., Palaniappan A., Zhang J., Liedberg B. Peptide functionalized gold nanoparticles with optimized particle size and concentration for colorimetric assay development: detection of cardiac Troponin I. *ACS Sens.*, 2016, **1**, P. 1416–1422.

[27] Liu L., Xia N., Liu H., Kang X., Liu X., Xue C., He X. Highly sensitive and label-free electrochemical detection of microRNAs based on triple signal amplification of multifunctional gold nanoparticles enzymes and redox-cycling reaction. *Biosens. Bioelectron.*, 2014, **53**, P. 399–405.

[28] Sun L., Liu D. Functional gold nanoparticle-peptide complexes as cell-targeting agents. *Langmuir*, 2008, **24**, P. 10293–10297.

[29] Morais T., Soares M.E., Duarte J.A., Soares L., Maia S., Gomes P., Pereira E., Fraga S., Carmo H., Bastos M.D.L. Effect of surface coating on the biodistribution profile of gold nanoparticles in the rat. *Eur. J. Pharm. Biopharm.*, 2012, **80**, P. 185–193.

[30] Nel A., Xia T., Mädler L., Li N. Toxic potential of materials at the nano level. *Science*, 2006, **311**, P. 622–627.

[31] Balasubramanian S.K., Yang L., Yung L.Y., Ong C.N., Ong W.Y., Yu L.E. Characterization, purification and stability of gold nanoparticles. *Biomaterials.*, 2010, **31**, P. 9023–9030.

[32] Pan Y., Neuss S., Leifert A., Fischler M., Wen F., Simon U., Schmid G., Brandau W., Jahnen-Dechent W. Size-dependent cytotoxicity of gold nanoparticles. *Small*, 2007, **3**, P. 1941–1949.

[33] Zhang G., Yang Z., Lu W., Zhang R., Huang Q., Tian M., Li L., Liang D., Li C. Influence of anchoring ligands and particle size on the colloidal stability and in vivo biodistribution of polyethylene glycol-coated gold nanoparticles in tumor-xenografted mice. *Biomaterials.*, 2009, **30**, P. 1928–1936.

[34] Sonavane G., Tomoda K., Makino K. Biodistribution of colloidal gold nanoparticles after intravenous administration: Effect of particle size. *Colloids and Surfaces B: Biointerfaces.*, 2008, **66**, P. 274–280.

[35] De. Jong W.H., Hagens W.I., Krystek P., Burger M.C., Sips A.J., Geertsma R.E. Paticle size-dependent organ distribution of gold nanoparticles after intravenous administration. *Biomaterials*, 2008, **29**, P. 1912–1919.

[36] Connolly M., Pérez Y., Mann E., Herradón .B, Fernández-Cruz M.L., Navas J.M. Peptide-biphenyl hybrid-capped AuNP, P. stability and biocompatibility under cell culture conditions. *Nanoscale Research Letters*, 2013, **8**, P. 315–323.

[37] Oberdorster G., Oberdorster E., Oberdorster J. Nanotoxicology: an emerging discipline evolving from studies of ultrafine particles. *Environ. Health Perspect.*, 2005, **113**, P. 823–839.

[38] Tedesco S., Doyle H., Redmond G., Sheehan D. Gold nanoparticles and oxidative stress in Mytilus edulis. *Marine Environmental Research*, 2008, **66**, P. 131–133.

[39] Schaeublin N.M., Braydich-Stolle L.K., Schrand A.M., Miller J.M., Hutchison J., Schlagera J.J., Hussain S.M. Surface charge of gold nanoparticles mediates mechanism of toxicity. *Nanoscale*, 2011, **3**, P. 410–420.

[40] Feng S., Ruanb G., Lic Q. Fabrication and characterizations of a novel drug delivery device liposomes-in-microsphere (LIM). *Biomaterials*, 2004, **25**, P. 5181–5189.

[41] Honary S., Zahir F. Effect of zeta potential on the properties of nano-drug delivery systems-A review (Part 2). *Tropical J. of Pharmaceutical Research*, 2013, **12**, P. 265–273.

Submitted 2 September 2024; revised 12 December 2024; accepted 23 December 2024

Information about the authors:

Sudeshna Kar – Assistant Professor, Department of Basic Science and Humanities (Chemistry), St. Thomas College of Engineering and Technology, 4, Diamond Harbour Rd, Alipore Body Guard Lines, Khidirpur, Kolkata, West Bengal 700023, Kolkata, India; ORCID 0000-0002-0469-3399; 06.sudeshna@gmail.com

Yian Tai – Professor, Department of Chemical Engineering, National Taiwan University of Science and Technology, 43 Keelung Road, Taipei-106, Taiwan; ORCID 0000-0001-7000-6086; ytai@mail.ntust.edu.tw

Conflict of interest: The authors do not have other competing interests to declare.

Declaration: No part of the manuscript has been published before.

Associated Content: Supporting Information: Detailed synthesis and characterization of peptides and gold nanoparticles. NMR, FT-IR, Mass spectra, UV, EDX analysis (PDF).